8-3-2006

Maximum A Posteriori Resampling of Noisy, Spatially Correlated Data

John A. Goff
University of Texas at Austin

Chris Jenkins
University of Colorado Boulder

Brian R. Calder
University of New Hampshire, Durham, brian.calder@unh.edu

Recommended Citation
Goff, J. A., C. Jenkins, and B. Calder (2006), Maximum a posteriori resampling of noisy, spatially correlated data, Geochem. Geophys. Geosyst., 7, Q08003, doi:10.1029/2006GC001297.

Geochemistry Geophysics Geosystems G3
AN ELECTRONIC JOURNAL OF THE EARTH SCIENCES
Published by AGU and the Geochemical Society

Article
Volume 7, Number 8
3 August 2006
Q08003, doi:10.1029/2006GC001297
ISSN: 1525-2027

Maximum a posteriori resampling of noisy, spatially correlated data

John A. Goff
University of Texas Institute for Geophysics, Jackson School of Geosciences, 4412 Spicewood Springs Road, Building 600, Austin, Texas 78759, USA (goff@ig.utexas.edu)

Chris Jenkins
Institute of Arctic and Alpine Research, University of Colorado, Campus Box 450, Boulder, Colorado, 80309-0450, USA

Brian Calder
Center for Coastal and Ocean Mapping and Joint Hydrographic Center, Chase Ocean Engineering Laboratory, University of New Hampshire, Durham, New Hampshire, 03824, USA

[1] In any geologic application, noisy data are sources of consternation for researchers, inhibiting interpretability and marring images with unsightly and unrealistic artifacts. Filtering is the typical solution to dealing with noisy data. However, filtering commonly suffers from ad hoc (i.e., uncalibrated, ungoverned) application. We present here an alternative to filtering: a newly developed method for correcting noise in data by finding the "best" value given available information. The motivating rationale is that data points that are close to each other in space cannot differ by "too much," where "too much" is governed by the field covariance. Data with large uncertainties will frequently violate this condition and therefore ought to be corrected, or "resampled." Our solution for resampling is determined by the maximum of the a posteriori density function defined by the intersection of (1) the data error probability density function (pdf) and (2) the conditional pdf, determined by the geostatistical kriging algorithm applied to proximal data values. A maximum a posteriori solution can be computed sequentially going through all the data, but the solution depends on the order in which the data are examined. We approximate the global a posteriori solution by randomizing this order and taking the average. A test with a synthetic data set sampled from a known field demonstrates quantitatively and qualitatively the improvement provided by the maximum a posteriori resampling algorithm. The method is also applied to three marine geology/geophysics data examples, demonstrating the viability of the method for diverse applications: (1) three generations of bathymetric data on the New Jersey shelf with disparate data uncertainties; (2) mean grain size data from the Adriatic Sea, which is a combination of both analytic (low uncertainty) and word-based (higher uncertainty) sources; and (3) side-scan backscatter data from the Martha's Vineyard Coastal Observatory which are, as is typical for such data, affected by speckle noise. Compared to filtering, maximum a posteriori resampling provides an objective and optimal method for reducing noise, and better preservation of the statistical properties of the sampled field. The primary disadvantage is that maximum a posteriori resampling is a computationally expensive procedure.

Components: 8250 words, 13 figures, 1 table.

Keywords: grain size; bathymetry; backscatter; filter.

Index Terms: 3252 Mathematical Geophysics: Spatial analysis (0500); 3265 Mathematical Geophysics: Stochastic processes (3235, 4468, 4475, 7857); 3045 Marine Geology and Geophysics: Seafloor morphology, geology, and geophysics.

Received 2 March 2006; **Revised** 16 May 2006; **Accepted** 9 June 2006; **Published** 3 August 2006.

Goff, J. A., C. Jenkins, and B. Calder (2006), Maximum a posteriori resampling of noisy, spatially correlated data, *Geochem. Geophys. Geosyst.*, *7*, Q08003, doi:10.1029/2006GC001297.

1. Introduction

[2] The presentation of data in spatial coordinates is an issue faced by nearly every geoscientist. Whether it is topography, geologic properties, geophysical data, or some other measurement collected as a function of x and y, a map of some sort typically must be generated for interpretation and analysis. In many such cases, data are noisy, producing artifacts that are a detriment both in presentation and interpretability. The common solution to problems of noisy data is to filter the data in some way. Filters are usually simple to apply and computationally efficient. However standard filtering techniques are typically ad hoc, in that the weighting function used to compute the average of neighboring values are defined by the user rather than by the intrinsic properties of the data. Also, filters are not straightforward to apply in situations where data are irregularly sampled in space, or where data of varying resolution are mixed; situations which will be important to the applications considered here.

[3] In this paper we present an alternative to filtering, which we term "maximum a posteriori resampling," which attempts to find the optimal value at each data location given the sample value at that location, its uncertainty, knowledge of proximal sample values and uncertainties, and an understanding of the true spatial covariance structure of the field. Qualitatively we know that, for any field that is not overly erratic (i.e., characterized by a red spectrum), two data samples that are close to each other in space should not differ by too much. Noisy data (i.e., data with large uncertainties) frequently violate this criterion, and the result is artifacts in the data. Quantitatively, we can define "too much" by the correlation properties of a field, which are used to establish the conditional probability density function (pdf) of one value given one or more proximal values, and which is functionally dependent on the lag distances between the points [e.g., *Feller*, 1971]: "too much" occurs when a data value is extremely improbable in terms of the conditional pdf determined by the proximal data values, and in such cases we desire to find an optimal correction for the wayward point.

[4] In any attempt to correct noisy data, better resolved data should count more than poorly resolved data, if that distinction can be made. There are numerous examples where data of varying quality are combined into a unified data set, commonly by merging older and newer data [e.g., *Jenkins*, 1997; *Jakobsson et al.*, 2002; *Calder*, 2006]. Quantitatively, data quality is determined by an uncertainty value, which expresses the root-mean square (rms) difference between the true value and measured value (true value plus measurement error). Where, for example, a well-constrained data value is close to a poorly constrained data value, the latter should be adjusted more than the former.

[5] Our basic operating assumption for maximum a posteriori resampling is that there are two independent probability density functions (pdfs) which characterize the data value at any one sample location: (1) the sample error pdf, with expected value and variance defined by the sample value and the square uncertainty, respectively, and (2) the conditional pdf, with expected value and variance derived from knowledge of the data values at proximal locations. In the Bayesian formulation, these pdfs act respectively as a priori, $p_a(Z)$, and conditional, $p_c(Z|Z_i)$, density functions in the formulation of an a posteriori density $p_p(Z)$, determined by the intersection or multiplication of the two [e.g., *Menke*, 1989, equation 5.9]:

$$p_p(Z) \propto p_a(Z)p_c(Z|Z_i), i \in 1, N, \quad (1)$$

where Z is the value of interest, Z_i are values sampled at N proximal locations, and assuming for the moment that there is no distribution associated with the Z_i values (i.e., that they are perfectly

sampled). The most probable (i.e., "best") value is given by the peak of the posterior density [*Menke*, 1989]. Maximum a posteriori resampling is a constrained estimate of the true value of the data at that point. However, because each Z_i also has an a priori sample error pdf, a global solution requires integration over the full data probability space [*Menke*, 1989, equation 5.10], which is analytically intractable for large data sets. We approximate the global solution with a Monte Carlo method described later. An understanding of both the data errors and the correlation statistics (i.e., covariance function, or semi-variogram) are required to implement this methodology. A comparable methodology is "projection onto convex sets," or POCS [e.g., *Weerasinghe et al.*, 2002], which is a general, iterative means for incorporating multiple a priori constraints into an estimation. Each constraint can be represented as a convex set in Hilbert space, and POCS seeks at least one point in the intersection of those sets by iteratively projecting onto each of the sets. The primary difference is that maximum a posteriori resampling seeks the best estimation, rather than just a valid one.

[6] In this paper we describe the maximum a posteriori resampling algorithm and test its effectiveness on a synthetic example, where the "true" field is known and artificially sampled with various uncertainties. We then apply the methodology to three examples from the coauthors' previous research: bathymetry on the Atlantic margin of the United States (Figure 1), mean grain sizes in the Adriatic Sea (Figure 2), and acoustic backscatter from the nearshore regions off Martha's Vineyard, Massachusetts (Figure 3).

[7] The region of the US Atlantic margin chosen for analysis contains data from three different sources [*Calder*, 2006]: fathometer data collected in the 1930s, echo-sounding values collected in the 1970s (both contained in the National Geophysical Data Center archives), and multibeam data collected in 1996 [*Goff et al.*, 1999]. Regions not constrained by multibeam data are marred by numerous "dimple" artifacts in the bathymetric interpolation (Figure 1). *Calder* [2006] conducted an error analysis of all three types of data and found that the fathometer data were substantially biased toward shallower values; the dimples in Figure 1 are, primarily, caused by these positive errors. While *Calder* [2006] in his rendering of the bathymetry in this region chose simply to remove the fathometer data as inconsistent with subsequent data, here we retain them in the data set to demonstrate the utility of the maximum a posteriori resampling methodology in mitigating such problems without a priori knowledge of their existence. Analysis of the spatial statistics of the bathymetry in this region was conducted by *Goff et al.* [1999] on the basis of the multibeam bathymetry.

[8] Mean grain sizes in the Adriatic sea (Figure 2) are presented by C. J. Jenkins and J. A. Goff (Competent interpolation for seabed substrates, with uncertainty calculations, submitted to *Continental Shelf Research*, 2006; hereinafter referred to as Jenkins and Goff, submitted manuscript, 2006) in a study of optimal interpolation techniques. These data are contained in the dbSEABED database [*Jenkins*, 1997; *Williams et al.*, 2003], and are derived from two primary sources: (1) analytic measurements of the grain size histogram, through settling tube, sedigraph and/or dry sieve techniques, and (2) conversion of word-based descriptions of bottom samples (e.g., gravel, sand, mud, silt, clay, muddy sand, silty clay, etc.) into quantitative estimates of mean grain size by applying fuzzy logic techniques. The word-based data contain, understandably, significant uncertainties compared with the analytic data (Jenkins and Goff, submitted manuscript, 2006). In the interpolated data set (Figure 2a), both positive and negative dimples, where data values have large differences with nearby data points, are common. Nevertheless, the word-based mean grain size values constitute the vast majority of data values in the dbSEABED databases; in the Adriatic in particular, there are less than 200 analytically derived mean grain size values versus more than 2000 word-based values. The word-based values cannot therefore simply be excluded without severely compromising coverage. Estimates of both the uncertainty in mean grain size data values and the semi-variogram structure of the Adriatic data set are presented by Jenkins and Goff (submitted manuscript, 2006).

[9] Acoustic backscatter data from the Martha's Vineyard Coastal Observatory (Figure 3) were presented by *Goff et al.* [2004a]. These data are responding to strong variations in seabed grain sizes associated with so-called "rippled scour depressions" [*Cacchione et al.*, 1984], or "sorted bed forms" [*Murray and Thieler*, 2004], that are oriented at a small angle to shore-normal. As with all such examples, this backscatter mosaic is highly speckled with noise (over 50% of the total variance, as will be demonstrated later). Unlike the previous two data examples, this data set is densely sampled everywhere, in this case entirely filling a grid with 6-m node spacing. Although maximum a posteriori resampling is less efficient in such circumstances, this example is instructive because it

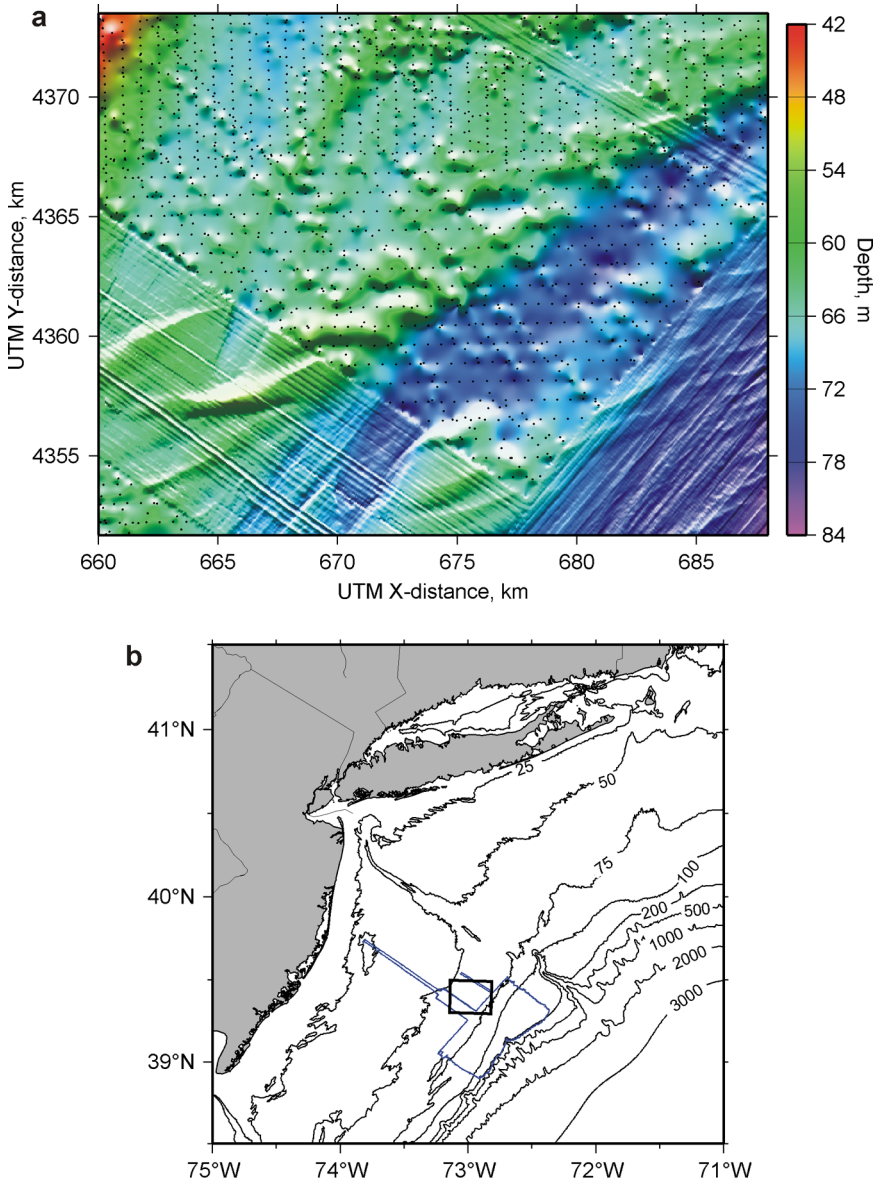

Figure 1. Bathymetric data from the New Jersey shelf [*Calder*, 2006]. (a) Region of data chosen for application of the maximum a posteriori resampling algorithm, color contoured and artificially illuminated from the north. Black dots indicate locations of archival fathometer and single narrow-beam data points from the National Geophysical Data Center. Striated regions are areas of multibeam bathymetry data [*Goff et al.*, 1999]; collocated archival data in this part of the grid were not used. Areas not covered by multibeam data were interpolated with a spline-in-tension algorithm [*Smith and Wessel*, 1990]. UTM x and y coordinates are for Zone 18. (b) Contoured bathymetry of the Mid-Atlantic Bight, indicating location of Figure 1a (box) and multibeam coverage (blue outline).

represents a situation where standard filtering techniques can be readily applied and thus compared quantitatively to our proposed methodology.

2. Method

2.1. The Two-Point Problem

[10] For illustrative purposes, we first consider the case of two data values μ_0 and μ_1 with large uncertainties, σ_0 and σ_1, respectively, that are sampled in spatial proximity to each other at locations X_0 and X_1, respectively (Figure 4). Assuming a normal distribution for the sample error, μ_0 and μ_1 also represent the means and σ_0^2 and σ_1^2 represent the variances for those distributions:

$$p_i(Z) = \frac{1}{\sqrt{2\pi}\sigma_i} \exp\left(\frac{-(Z-\mu_i)^2}{2\sigma_i^2}\right). \quad (2)$$

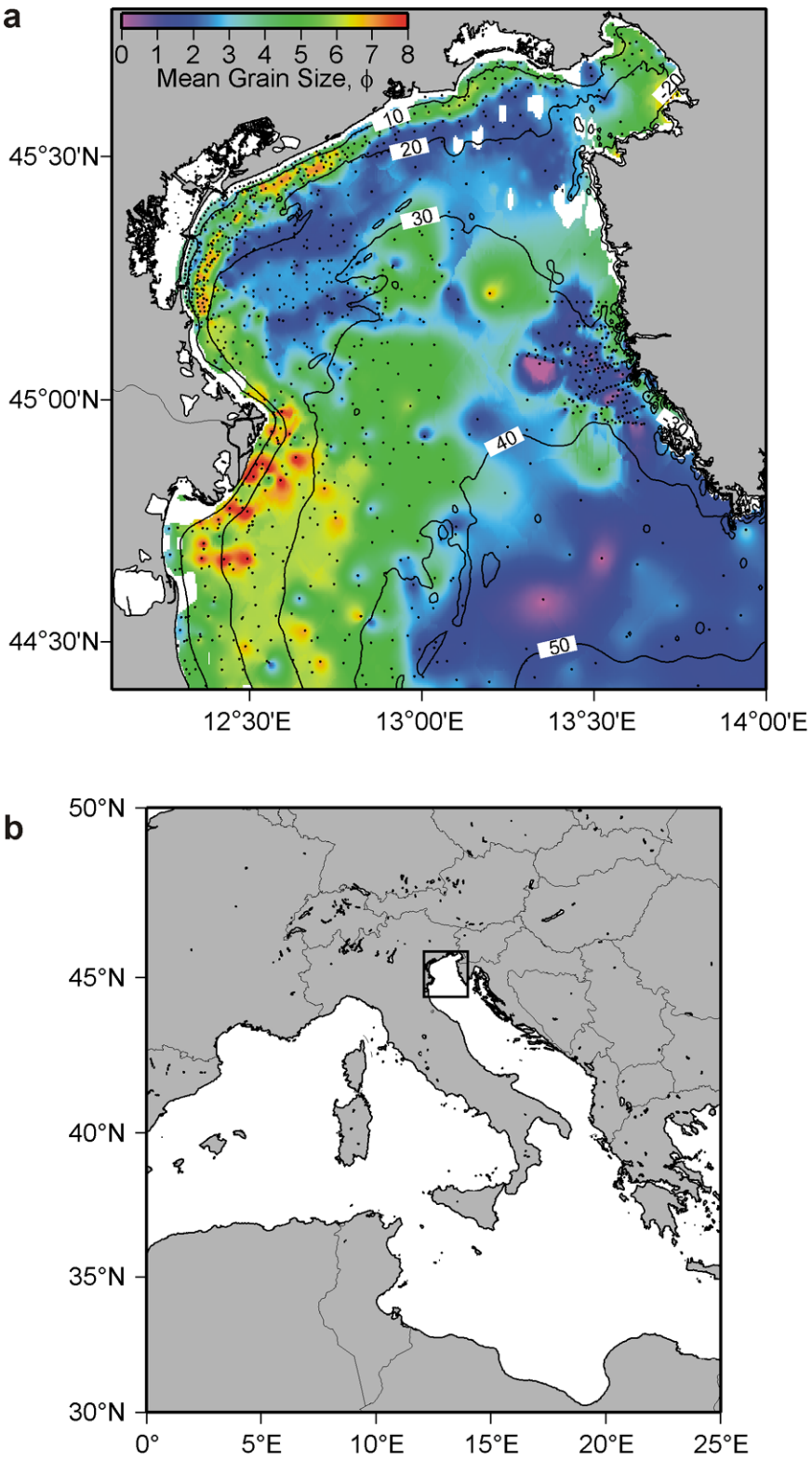

Figure 2. Mean grain sizes (in ϕ values, where grain size in mm is $2^{-\phi}$) in the Adriatic Sea (Jenkins and Goff, submitted manuscript, 2006). (a) Region of data chosen for application of the maximum a posteriori resampling algorithm, color contoured. Bathymetric contours in meters are also shown. Interpolation is accomplished through a modified version of the kriging algorithm (see text). (b) Geographic map of Mediterranean Sea indicating location of Figure 2a (box).

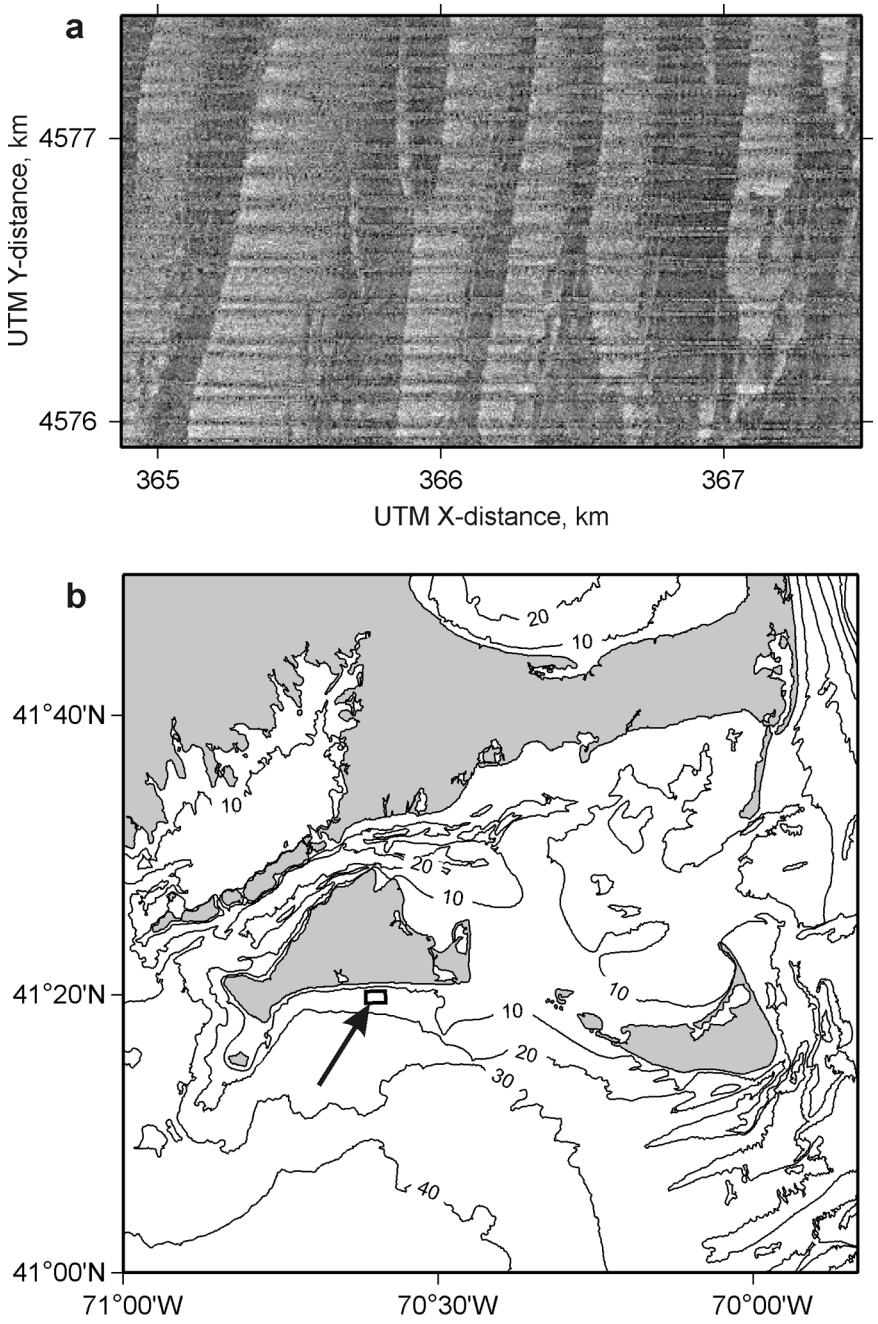

Figure 3. Acoustic backscatter in the nearshore regions (~12–16 m) of the Martha's Vineyard Coastal Observatory, Massachusetts [*Goff et al.*, 2004a]. (a) Section of backscatter chosen for application of the maximum a posteriori resampling algorithm. Lighter shades indicate higher backscatter intensity. UTM x and y coordinates are for Zone 19. (b) Contoured bathymetry (meters) of the waters south of Cape Cod, indicating location of Figure 3a (box with arrow).

If the data were sampling a white noise process, then values at locations X_0 and X_1 would be uncorrelated and the error pdfs would represent complete statistical descriptions of the data. However, in the more realistic case of a red-spectrum process, the values at these two locations are correlated, and a complete description of the data must include a conditional pdf for one data value given the other. This function provides additional information on the error structure of the data value.

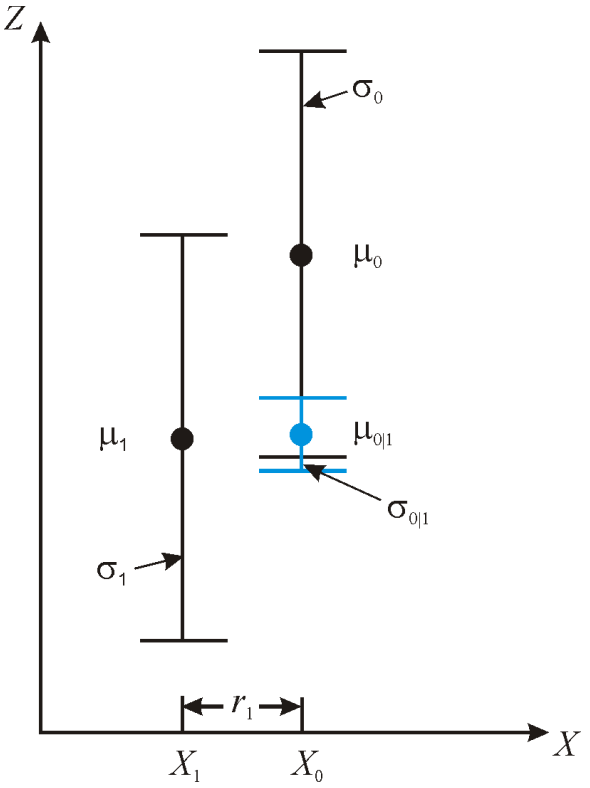

Figure 4. Illustration of the two-point problem of noisy, correlated data in proximity. Values μ_0 and μ_1 represent data values at locations X_0 and X_1, with uncertainties σ_0 and σ_1, respectively. The conditional expected value and uncertainty at X_0 given the value μ_1 at X_1 are represented by $\mu_{0|1}$ and $\sigma_{0|1}$, respectively. Where errors are large, the data value μ_0 may be incompatible with the conditional expectation and uncertainty, in which case it needs to be adjusted, or "resampled."

[11] First we assume, for the two-point problem illustrated in Figure 4, that the value at location X_1 is known to be μ_1 (which can also be thought of as the unconditional maximum a posteriori solution at X_1). We assume as well that the field is statistically homogeneous, that the covariance between the two locations, specified by $C(r_1)$, where $r_1 = |X_1 - X_0|$, is known, and that the mean is 0 or has been subtracted from the data. The covariance is further broken down via:

$$C(r_1) = H^2\rho(r_1), \tag{3}$$

where H^2, a constant, is the variance $C(0)$, and ρ is the correlation function dependent only on the lag distance. The conditional probability density $p_{0|1}(Z)$ at X_0 given the value μ_1 is a Gaussian function defined by the conditional mean

$$\mu_{0|1} \cong E[\mu_0|\mu_1] = \rho(r_1)\mu_1, \tag{4}$$

and conditional variance

$$\sigma^2_{0|1} \cong E\left[\left(\mu_0 - \mu_{0|1}\right)^2\right] = H^2\left(1 - \rho^2(r_1)\right) \tag{5}$$

[e.g., *Feller*, 1971]. The operator $E[a]$ is the expected value of a, and $E[a|b]$ is the expected value of a given b. The conditional pdf for location X_0 given the value μ_1 at X_1 is independent of the sample error pdf.

[12] Where the difference between μ_0 and μ_1 is large, and the lag distance r_1 between X_0 and X_1 is small, then we are likely to encounter the situation illustrated in Figure 4, where the data value μ_0 is highly unlikely given the conditional pdf defined by $\mu_{0|1}$ and $\sigma_{0|1}$. In this case, the data value does not represent the best possible estimate of the value at location X_0; rather, we seek a value that is most probable given both pdfs that independently describe the error space. This is accomplished by finding the maximum of the a posterior density defined by the intersection of the sample error pdf and the conditional pdf [*Menke*, 1989] (Figure 5). This value, $\mu^m_{0|1}$, is derived as the zero first derivative of the multiplication of the two Gaussian pdfs, the solution

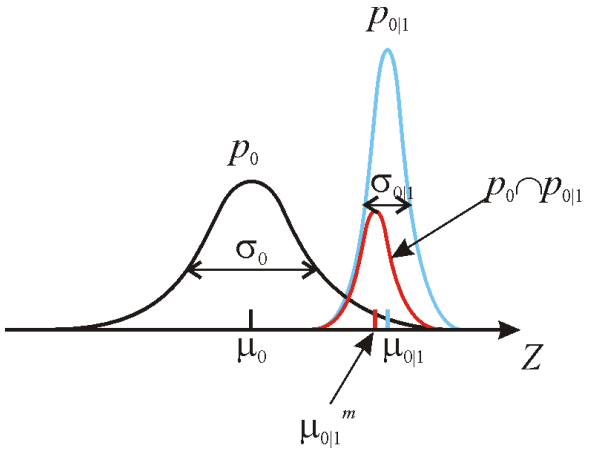

Figure 5. Illustration of the a posteriori function at location X_0 (Figure 4) as the intersection of the a priori (p_0) and conditional ($p_{0|1}$) probability density functions. The maximum a posteriori value is indicated by $\mu_{0|1}{}^m$. See text for discussion and complete description of parameters.

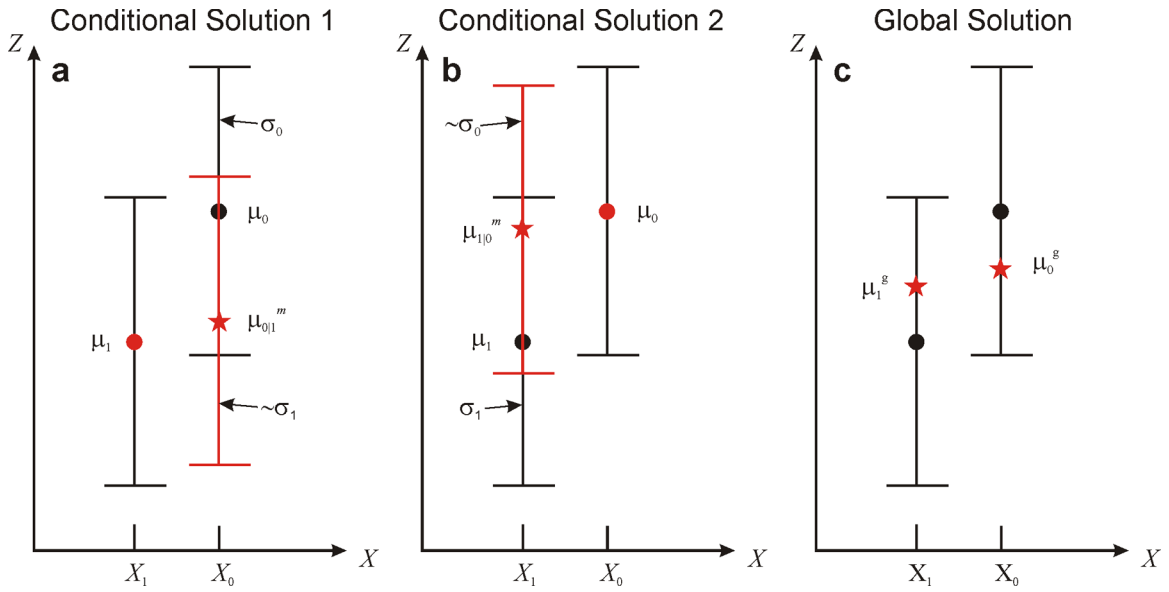

Figure 6. Illustration of non-uniqueness of the maximum a posteriori resampling procedure for the two-point problem. (a) The maximum of the a posteriori density, $\mu_{0|1}{}^m$, at location X_0 assuming the value at location X_1 is μ_1. The uncertainty in this solution, given the probability density of possible values at X_1, is approximately σ_1. (b) The maximum of the a posteriori density, $\mu_{1|0}{}^m$, at location X_1 assuming the value at location X_0 is μ_0. The uncertainty in this solution, given the probability density of possible values at X_0, is approximately σ_0. (c) The global maximum a posteriori values at each location, $\mu_0{}^g$ and $\mu_1{}^g$, are determined by equations (7) and (8), respectively.

of which, written in a way that emphasizes the weighting factors, is

$$\mu_{0|1}^m = \frac{\mu_0\sigma_0^{-2} + \mu_{0|1}\sigma_{0|1}^{-2}}{\sigma_0^{-2} + \sigma_{0|1}^{-2}}. \quad (6)$$

In other words, the conditional maximum a posteriori solution is the average of the two means weighted by their precisions, which are proportional to the inverse of their respective variances.

[13] The maximum a posteriori solution for the two-point problem (equation (6)) is, of course, non-unique. If the RMS errors for the two values are equal, then with equal probability we could have assumed that the value at X_0 were known to be μ_0 and solved for the maximum a posteriori solution, $\mu_{1|0}^m$, at location X_1. There are thus two conditional maximum a posteriori solutions, as illustrated in Figure 6. These solutions are determined by the sequence in which we resample the data points, which will be a critical factor in addressing the multiple-point problem in the next section.

[14] We could, in fact, assume as known, although with lesser probability and therefore not as a "maximum" a posteriori solution, any value from within the sample error pdfs at the two locations. A global maximum a posteriori solution requires the integration of these solutions over the data probability space [e.g., *Menke*, 1989, equation 5.10]. A useful shortcut, however, is possible by noting that there are two "solution" pdfs at each location (Figure 6): one determined simply by the range of values that can be assumed at a location from the sample error pdf, and the other determined from the range of values computed by the maximum a posteriori formulation of equation (6), where a value is first assumed at the alternate location. For example, at X_0 we have, as pdfs for the solution at that location (Figure 6a), the sample error pdf $p_0(Z)$, with mean μ_0 and variance σ_0^2, and the mapping of the error distribution at X_1 onto X_0 via equation (6), $p_{0|1}^m(Z)$, with mean $\mu_{0|1}^m$ and variance of $\sim\sigma_1^2$ if X_1 and X_0 are close to each other. The global maximum a posteriori solution at both locations, μ_0^g and μ_1^g (Figure 6c), can thus be determined from zero first derivative of the multiplication of the two solution pdfs at each location:

$$\mu_0^g \approx \frac{\mu_0\sigma_0^{-2} + \mu_{0|1}^m\sigma_1^{-2}}{\sigma_0^{-2} + \sigma_1^{-2}}, \quad (7)$$

$$\mu_1^g \approx \frac{\mu_1\sigma_1^{-2} + \mu_{1|0}^m\sigma_0^{-2}}{\sigma_0^{-2} + \sigma_1^{-2}}. \quad (8)$$

In other words, the global maximum a posteriori solution is the average of all possible conditional maximum a posteriori solutions, weighted by the probability of their occurrence.

2.2. Multiple-Point Solution

[15] The maximum a posteriori solution to the multiple-point problem requires first that a sequence be established among the data values to be resampled, so that the maximum a posteriori value determined at any one point is conditioned on all the maximum a posteriori solutions determined at the prior points in the sequence. This is necessary to ensure internal consistency; i.e., that the solution at one location is similar to the solution at a proximal location. The algorithm would begin at the first location in the sequence, where the value is assumed to be the data point sampled at that location (which is the maximum a posteriori solution with no other conditions). At the second location in the sequence, the maximum a posteriori value is determined from the sample error pdf and the conditional pdf calculated from the maximum a posteriori solution at the first location (i.e., the two-point solution of equation (6)). At the third location, the maximum a posteriori value is determined from the sample error pdf and the conditional pdf calculated from the maximum a posteriori solutions at the prior two locations, and so on. This procedure has close affinity with the classic geostatistical method of sequential Gaussian simulation (SGS) [e.g., *Deutsch and Journel*, 1992], in which a value at an unsampled location is selected from the pdf conditioned both on sampled data values and on values simulated earlier in the sequence.

[16] As we found with the two-point problem, the conditional maximum a posteriori solution is strongly dependent on the sequence of points chosen for resampling; i.e., it is non-unique, with the number of possible solutions expanding geometrically with the number of data points. A closed form solution for the global maximum a posteriori solution, such as expressed in equations (7) and (8) for the two-point problem, quickly becomes intractable as the number of data points increases. However, by inference from the 2-point solution (equations (7) and (8)), where we determined that the global maximum a posteriori solutions is the average of conditional solutions weighted by the probability of each, we surmise that a global solution can be approached through a Monte Carlo method of averaging a number of solutions that are sampled from the solution probability space. Such solutions can be generated through construction of random resampling sequences, where the choice of the next location in the sequence is weighted by the probability (proportional to the inverse of the error variance) of that sample value. For example, in the 2-point problem (Figure 4), we could accurately estimate the global maximum a posteriori value using a Monte Carlo method by choosing to start with either μ_0 or μ_1 as the initial condition with probability proportion to the inverse of the error variance of each, leading to one or the other of the two conditional solutions illustrated in Figure 6. After generating a large number of such Monte Carlo solutions, the average will approach the analytic solutions of equations (7) and (8).

[17] Our algorithm for approximating the multiple-point global maximum a posteriori value proceeds as follows. Let the data consist of point tuples (X_i, Y_i, μ_i), $1 \le i \le N$, and for simplicity, consider the locations as vectors $\mathbf{X}_i = (X_i, Y_i)$ giving ordered but arbitrarily indexed pairs ($\mathbf{X}_i$, μ_i). The sample sites are visited in a sequence chosen at random without replacement from the index set $\Omega = \{1, \ldots, N\}$ (i.e., as a (weighted) permutation of Ω), giving an index sequence of $\mathbf{S}_N = (S_1, \ldots, S_N)'$, with properties $S_i \in \Omega$, $S_i \neq S_j$, $1 \le i \ne j \le N$. The sequence is generated stepwise. Let $\mathbf{S}_n = (S_1, \ldots, S_n)'$ be the sequence up to the n-th site, and let $\mathbb{R}_n = \Omega \backslash \{S_i, 1 \le i \le n\} = \{R_i, 1 \le i \le N - n\}$ be the set of indices yet to be chosen; i.e., the remainder set.

[18] The next site for resampling is chosen by selecting S_{n+1} from $\mathbb{R}_n$ in a probabilistic manner, weighted by the probability of sample values among the remainder set. We first assign a probability mass to the remainder set:

$$p_n\{R_i\} = W_n^{-1}\sigma_{R_i}^{-2}, 1 \le i \le N - n, \tag{9}$$

$$W_n = \sum_{i=1}^{N-n} \sigma_{R_i}^{-2}, \tag{10}$$

where σ_{R_i} is the sample error of μ_{R_i}. The cumulative distribution is

$$P_n\{R_k\} = \sum_{i=1}^{k} p_n\{R_i\}, 1 \le k \le n, \tag{11}$$

and S_{n+1} is determined by selecting a random value, *Ran*, from a uniform distribution on (0,1], and assigning $S_{n+1} = R_k$, where $P_n(R_{k-1}) < Ran \le P_n(R_k)$. The sequence is then updated: $\mathbf{S}_{n+1} = (S_1, \ldots, S_n, S_{n+1})'$, $\mathbb{R}_{n+1} = \mathbb{R}_n \backslash S_{n+1}$. The critical attribute

of this sequencing algorithm is that data values with lower uncertainties will tend to be chosen earlier in the sequence than data values with greater uncertainties, and in this way exert greater influence on the Monte Carlo global solution described below.

[19] As with SGS, the maximum a posteriori resampling algorithm employs kriging [e.g., *Cressie*, 1990] to compute the conditional mean $\mu_{S_{n+1}|\mathbf{S}_n}$ and variance $\sigma_{S_{n+1}|\mathbf{S}_n}{}^2$ at the latest location in the sequence given estimates at prior locations in the sequence; i.e., the multipoint equivalent of equations (4) and (5). These equations are

$$\mu_{S_{n+1}|\mathbf{S}_n} = \mathbf{c}_n' \mathbf{C}_n^{-1} \mathbf{Z}_n \tag{12}$$

$$\sigma^2_{S_{n+1}|\mathbf{S}_n} = H^2 - \mathbf{c}_n' \mathbf{C}_n^{-1} \mathbf{c}_n, \tag{13}$$

where $\mathbf{Z}_n = (\mu_{S_1}{}^m, \mu_{S_2}|\mathbf{S}_1{}^m, \ldots, \mu_{S_n}|\mathbf{S}_{n-1}{}^m)'$ are the previous resampled values in the sequence, $\mathbf{c}_n = (C(\|\mathbf{X}_{S_{n+1}} - \mathbf{X}_{S_1}\|), \ldots, C(\|\mathbf{X}_{S_{n+1}} - \mathbf{X}_{S_n}\|))'$, and $\mathbf{C}_n$ is an $n \times n$ covariance matrix with $C_{ij} = C(\|\mathbf{X}_{S_i} - \mathbf{X}_{S_j}\|)$. In practice, inverting $\mathbf{C}_n$ for large n is problematic, and we avoid the issue by limiting the solution to the 10 nearest neighbors of S_{n+1} in $\mathbf{S}_n$. Such limitations are common practice in kriging and SGS [e.g., *Deutsch and Journel*, 1992], and justified in such cases as the von Kármán spectral model [e.g., *Goff and Jordan*, 1988] which satisfy the criteria for being pseudo-Markovian [*Adler*, 1981, p. 259].

[20] The conditional maximum a posteriori solution at $\mathbf{X}_{S_{n+1}}$ is given by

$$\mu^m_{S_{n+1}|\mathbf{S}_n} = \frac{\mu_{S_{n+1}}\sigma^{-2}_{S_{n+1}} + \mu_{S_{N+1}|\mathbf{S}_n}\sigma^{-2}_{S_{n+1}|\mathbf{S}_n}}{\sigma^{-2}_{S_{n+1}} + \sigma^{-2}_{S_{n+1}|\mathbf{S}_n}}, \tag{14}$$

where $\mu_{S_{n+1}}$ is the sample data value and $\sigma_{S_{n+1}}$ is the RMS error at $\mathbf{X}_{S_{n+1}}$. This solution is, as we have previously noted, non unique, dependent on the chosen random sequence $\mathbf{S}_N$. However, by construction of the sequence, each value for $\mu_{S_{n+1}}|\mathbf{S}_n{}^m$ is a random sample taken from the pdf for $\mu^g_{S_{n+1}}$, the global maximum a posteriori solution at $\mathbf{X}_{S_{n+1}}$. The average of many such $\mu^m_{S_{n+1}|\mathbf{S}_n}$ values will therefore provide an approximation for $E[\mu^g_{S_{n+1}}]$. This convergence is guaranteed by the central limit theorem [e.g., *Taylor and Karlin*, 1984, p. 27], which states that the sum $Z_n = z_1 + z_2 + \ldots + z_n$ of identically distributed summands $z_1, z_2, \ldots, z_n$, having finite mean $\mu = E[z_k]$ and variance $\sigma^2 = \mathrm{Var}[z_k]$, is, for large n, approximately normally distributed with mean $n\mu$ and variance $n\sigma^2$. The average therefore will have mean μ and vanishingly small variance σ^2/n. More formally, we specify a set of independent sequences $\mathbb{S}_M = \{\mathbf{S}_{N,m}, 1 \le m \le M\}$ giving rise to a set of solution vectors $\mathbb{Z}_M = \{\mathbf{Z}_{N,m}, 1 \le m \le M\}$ whose N ordered elements are the full set of solutions to equation (14) for each sequence in $\mathbb{S}_M$. The vector $\mathbf{Z}_g$ of expected values at all points for the global maximum a posteriori solution are then estimated by

$$\mathbf{Z}_g = M^{-1} \sum_{m=1}^{M} \mathbf{Z}_{N,m}. \tag{15}$$

In applications such as those reported here, a typical choice for stable estimation of $\mathbf{Z}_g$ is $M = 20$ sequences.

3. Test on Synthetic Data

[21] To test the capabilities of the maximum a posteriori resampling algorithm, we apply it to "data" samples taken from a fully realized synthetic field (Figure 7a). This "unconditional realization" is generated with a spectral method from a von Kármán statistical model [e.g., *Goff and Jordan*, 1988]. The von Kármán model in one dimension is parameterized by three values: the RMS variability, H, the correlation scale, λ, and the fractal dimension, D. In two dimensions, the lateral scale is allowed to vary ellipsoidally, with parameters λ_n and λ_s being the correlation scales normal to and along the strike direction, respectively, and θ_s being the orientation of the strike direction. The field generated in Figure 7a is isotropic, with $H = 1.0$, $\lambda_n = \lambda_s = 2.8$ (units are arbitrary), and $D = 2.2$, with a grid size of 1001 $\times$ 1001 points and a node spacing of 0.01 in both the x and y directions. Under artificial illumination, the synthetic field appears as a fairly realistic simulation of a topographic surface.

[22] The synthetic surface was "sampled" at 1000 points whose x and y indices were chosen at random from uniform distributions over the horizontal and vertical ranges of the grid, respectively, and then interpolated with a spline in tension algorithm [*Smith and Wessel*, 1990] to generate a predicted surface. The randomness of the locations of sample points is not essential to this test; data points are never "randomly" selected. More important is that some locations are clustered whereas others are isolated, which

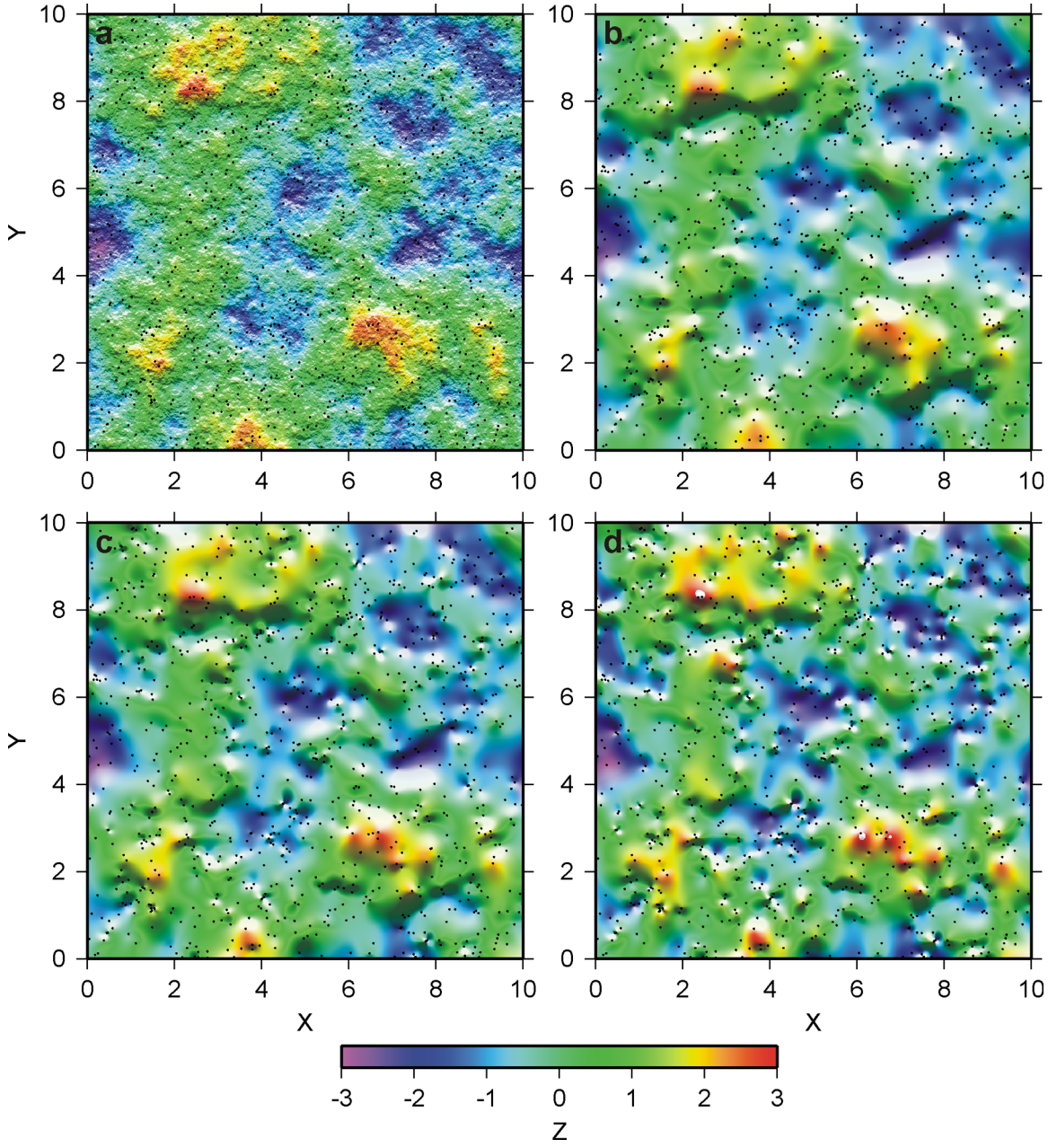

Figure 7. (a) Realization of the von Kármán statistical model [e.g., *Goff and Jordan*, 1988], generated using parameters RMS height (H) = 1.0, isotropic correlation scales ($\lambda_n = \lambda_s$) = 2.8, and fractal dimension (D) = 2.2. Vertical and horizontal scale units are arbitrary. Black dots indicate locations where field has been sampled for subsequent images. (b) Interpolated field from perfect samples of Figure 7a. (c) Interpolated field from samples of Figure 7a with a random uncertainty of 0.2. (d) Interpolated field from samples of Figure 7a with a random uncertainty of 0.5. All images are color contoured and artificially illuminated from the north. Interpolations employ a spline-in-tension algorithm [*Smith and Wessel*, 1990].

is typical for data of mixed generations. The locations indicated in Figure 7a are suitable for this purpose. In Figure 7b, the values were sampled with no noise (i.e., perfect sampling). A random Gaussian noise value was added in Figures 7c and 7d, with RMS values of 0.2 and 0.5, respectively. Table 1 lists the overall RMS error between each of these three prediction surfaces and the "true" surface. As the amount of noise in the data increases, the prediction error also increases, and the image of the surface

Table 1. RMS Error Between the Synthetic Surface (Figure 7a) and the Prediction Surfaces Generated by Interpolating From Sample Points, With Specified Sample Error, Both Before and After Resampling

Sample Error	Before Resampling	After Resampling
0	0.25	NA
0.2	0.30	0.28
0.5	0.50	0.37

degrades with increased severity of "dimple" artifacts.

[23] The maximum a posteriori resampling algorithm was written in Fortran code, and run on a Sun Ultra 10 workstation. The kriging procedure to determine conditional mean and variance at each point in the sequences was restricted to using the nearest 10 locations of previously resampled values. Here, a simple brute-force method was used for identifying the 10 nearest locations (applications described below required a more sophisticated search algorithm to reduce run time), and 20 independently generated sequences were used to compute a set of conditional maximum a posteriori solutions, which were then averaged to estimate the global maximum a posteriori solution. The full run time for this example was 20s.

[24] Interpolations of the resampled noisy values are presented in Figures 8a (for 0.2 RMS noise) and 8b (for 0.5 RMS noise). As desired, the dimple artifacts have been greatly diminished in these images, although not entirely eradicated in the higher noise case. Furthermore, as demonstrated in Table 1, the overall accuracy of the prediction surfaces has been improved by the maximum a posteriori resampling, substantially so in the higher noise case. Residuals between the original prediction surfaces (Figures 7c and 7d, respectively) and these post-resampling prediction surfaces are displayed in Figures 8c and 8d, respectively, demonstrating in detail the actual effect of the resampling algorithm. Changes to the prediction surface in the low noise case (Figure 8c) are mostly minimal, concentrating on the relatively few locations where significant incompatibilities between proximal points exist. Changes to the prediction surface in the high noise case (Figure 8d) are much more significant across the sample region. In other words, the maximum a posteriori resampling algorithm modified the sample values only slightly in the case where little correction was needed, and much more significantly where a lot of correction was needed. By all the measures noted above, the maximum a posteriori resampling algorithm was successful at its intended application.

4. Data Examples

[25] In this section we apply the maximum a posteriori resampling algorithm to three disparate types of marine data sets: bathymetry on the New Jersey shelf [*Goff et al.*, 1999; *Calder*, 2006], mean grain size in the Adriatic Sea (Jenkins and Goff, submitted manuscript, 2006), and acoustic backscatter in the coastal waters off Martha's Vineyard, Massachusetts [*Goff et al.*, 2004a].

[26] In the application of the maximum a posteriori resampling algorithm to two of the data examples, the number of data values is very large (>100,000) and the data density is high. In these circumstances, a brute force search for the nearest resampled values in the kriging step of the algorithm becomes untenable. To speed up the search process, we devised a sector search algorithm. Each data location is first assigned to a small sector, in this case a 5×5 subgrid of the main grid that establishes the boundaries of the data field. After a data value has been resampled, its location and value are stored in a list assigned to each sector. When kriging a new data location, the lists of resampled values from its sector and the 8 adjacent sectors are first searched. If the number of desired kriging locations is found, then the search is stopped. Otherwise the next "ring" of sector lists is searched, and so on until that number is found.

4.1. New Jersey Shelf Bathymetry

[27] The bathymetric data from the New Jersey shelf (Figure 1) are derived from three different sources [*Calder*, 2006]: fathometer data collected in the 1930s, vertical beam acoustic data collected in the 1970s, and multibeam data collected in 1996. The data were placed within a grid with node spacing of 50 m. Multibeam data were favored wherever an older data value fell within the same grid cell as a multibeam data value. The total number of data points in the grid considered is over 100,000, the vast majority of which are derived from the multibeam data which mostly fill the grid where such data are present. Elsewhere the grid is interpolated between data locations using a spline-in-tension algorithm [*Smith and Wessel*, 1990]. Numerous large dimple artifacts are present in regions that are not covered by multibeam data, owing primarily to the limited precision and shallow bias of the older fathometer data. The multi-

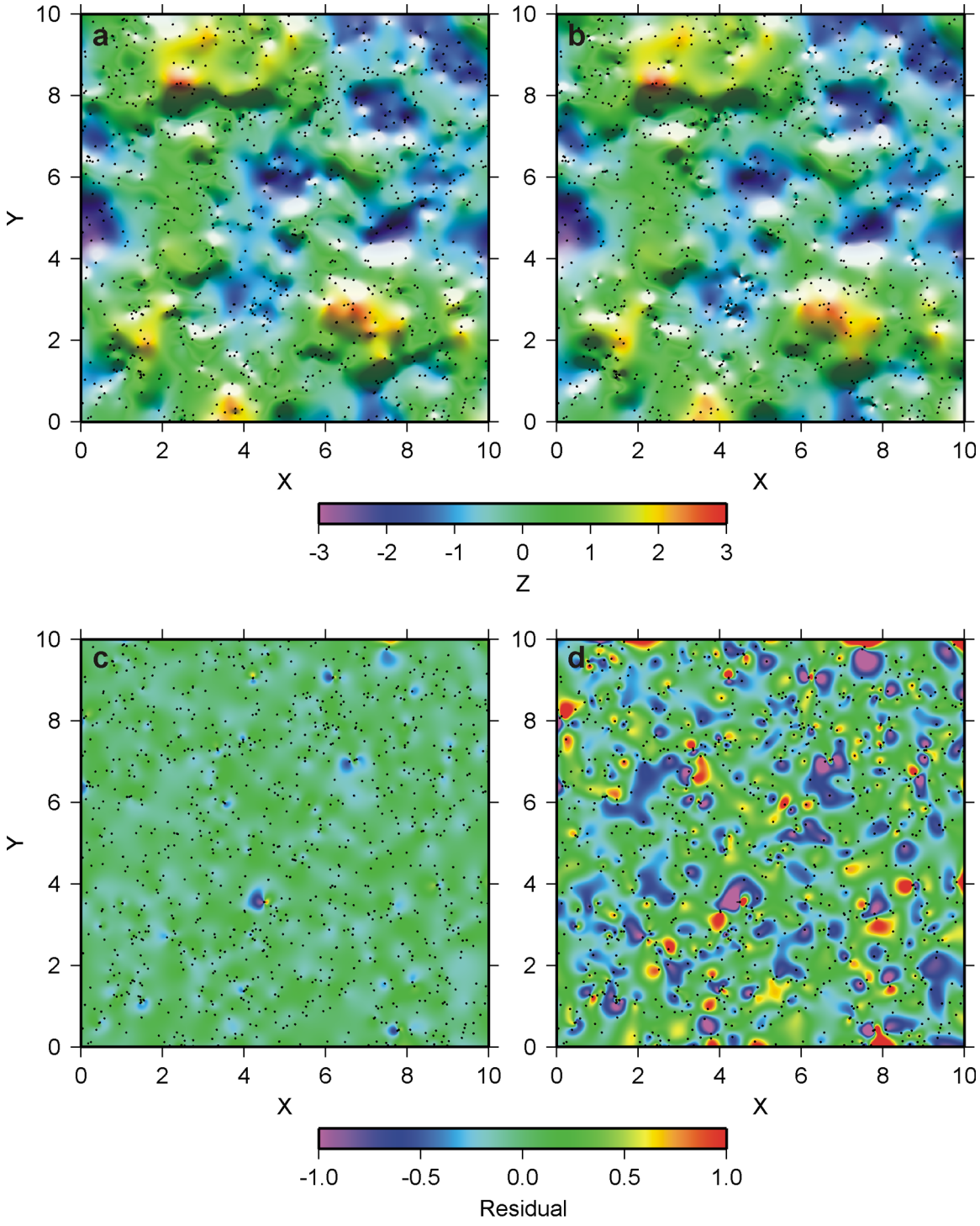

Figure 8. (a) Interpolation of synthetic data with 0.2 uncertainty (Figure 7c) after maximum a posteriori resampling. (b) Interpolation of synthetic data with 0.5 uncertainty (Figure 7d) after maximum a posteriori resampling. Interpolated images are color contoured and artificially illuminated from the north. Interpolations employ a spline-in-tension algorithm [*Smith and Wessel*, 1990]. (c) Color-contoured residual between pre-resample (Figure 7c) and post-resample (Figure 8a) interpolated images for 0.2 uncertainty. (d) Color-contoured residual between pre-resample (Figure 7d) and post-resample (Figure 8b) interpolated images for 0.5 uncertainty.

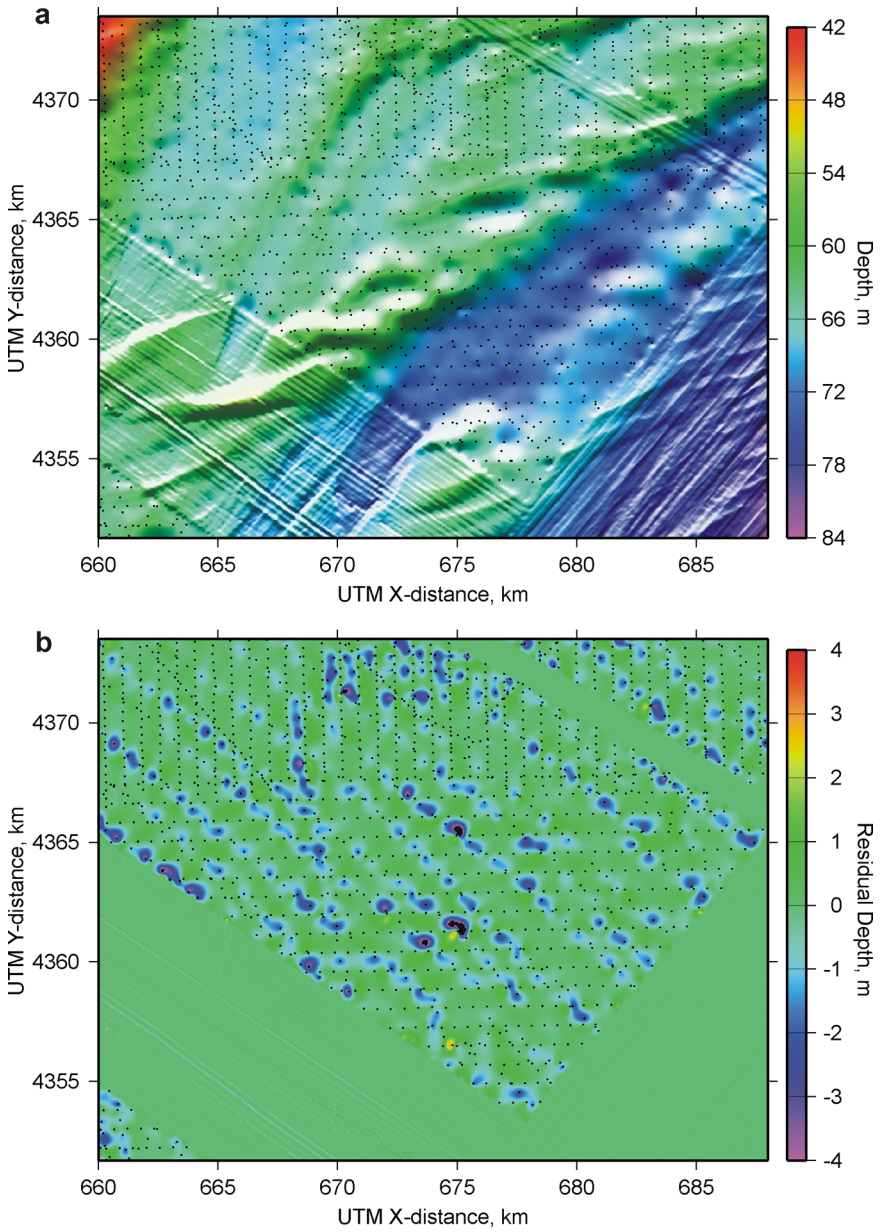

Figure 9. (a) Interpolation of New Jersey bathymetric data (Figure 1a) after maximum a posteriori resampling. Image is color contoured and artificially illuminated from the north. Black dots indicate locations of archival fathometer and single narrow-beam data points from the National Geophysical Data Center. Location shown in Figure 1b. (b) Color-contoured residual between pre-resampled (Figure 1a) and post-resampled (Figure 9a) interpolated images of the New Jersey bathymetry data.

beam data are also streaked by track line artifacts associated primarily with imperfect assessment of the water column sound speed structure [*Goff et al.*, 1999].

[28] *Calder* [2006] has analyzed the uncertainties in these different data sets: ~2 m for the fathometer data, ~0.5 m for the vertical beam acoustic data, and ~0.1–0.4 m for the multibeam data, which is functionally dependent on the beam angle. *Goff et al.* [1999] computed the covariance statistics of the sand ridge morphology, which is the dominant geomorphology in the region. For the area shown in Figure 1, suitable von Kármán covariance model parameters are: $H = 2.7$ m, $\lambda_n = 1.3$ km, $\lambda_s = 6.0$ km, $\theta = 70°$, and $D = 2.0$. Application of the maximum a posteriori resampling algorithm on this data set, incorporating the sector search algorithm for the 10 nearest resampled values for kriging, had a run time of ~2 hours on a Sun Ultra 10 workstation

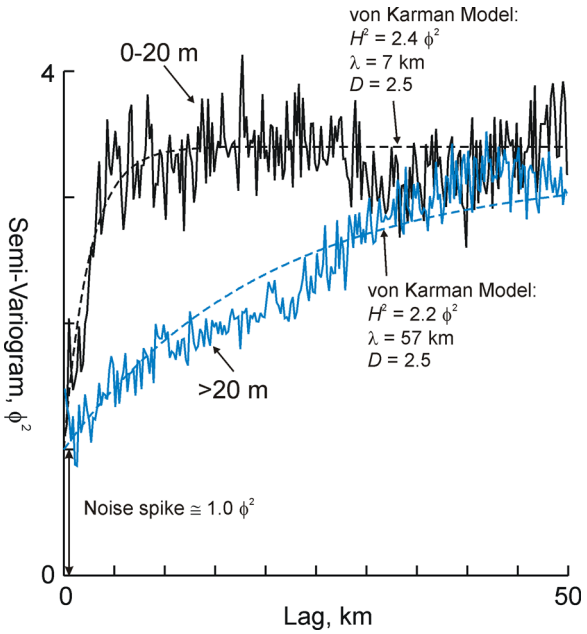

Figure 10. Semi-variograms computed for the mean grain size data set in 0–20 m and >20 m water depth ranges in the Adriatic Sea (adapted from Jenkins and Goff (submitted manuscript, 2006)). One-dimensional von Kármán statistical models are matched to each, with parameters as indicated. Both semi-variograms exhibit a white noise spike (the difference between the 0th and 1st lag) of ~1.0 ϕ^2.

(a brute force search would have taken at least a full day).

[29] The image generated from the resampled data values is presented in Figure 9 along with the residual values between the pre-resampling (Figure 1a) and post-resampling images. The dimple artifacts evident in Figure 1a are largely absent in the post-resampled image (Figure 9a), and the primarily negative residuals (Figure 9b) demonstrate that most of these artifacts are positive in nature, consistent with the bias of the fathometer data [*Calder*, 2006]. As evidenced by the subtle lineaments within multibeam portions of the residual image, some minor adjustments were made to the multibeam track line artifacts by the maximum a posteriori resampling algorithm. However, the net effect to reducing these artifacts in the post-resampling image (Figure 9a) is negligible. This failure is due to the fact that track line artifacts are highly correlated in nature, and therefore do not result in differences between proximal values that are highly inconsistent with the statistical nature of the field.

4.2. Adriatic Sea Mean Grain Size

[30] The mean grain sizes in the Adriatic Sea (Figure 2a) were derived from the global dbSEABED database [*Jenkins*, 1997; *Williams et al.*, 2003], and expressed as logarithmic ϕ values where the grain size in mm = $2^{-\phi}$. As described earlier, these values are derived from two different methods: (1) analytic evaluation of the grain size histogram using settling tube or sieve methods and (2) conversion of word-based descriptions to grain size estimates. There are ~200 analytic values, and over 2000 word-based values in the database for the Adriatic Sea. Uncertainties for analytic methods of mean grain size estimation are less than ~0.2 ϕ [e.g., *Goff et al.*, 2004b]. Uncertainties for the word-based data in the Adriatic Sea appear to be ~1.0 ϕ (Jenkins and Goff, submitted manuscript, 2006), or ~30–40% of the total data variance. This is demonstrated in Figure 10, where two independent semi-variograms constructed from the data are matched well by von Kármán model curves that intersect the 0-lag axis at a value of 1.0 ϕ^2, which is indicative of the noise spike.

[31] Also demonstrated in Figure 10 is the inhomogeneous nature of the data, where nearshore data (<20 m water depth) exhibit a much shorter correlation scale than offshore data (here we consider only the isotropic form of the covariance owing to the sparsity of the data). Experimentation with different depth ranges for computing the semi-variogram demonstrates that this transition is constrained to within ~5 m water depth of the 20 m contour. This change in the correlation properties is an important consideration both for the maximum a posteriori resampling algorithm and for interpolating the data values, because the level of predictability at one location given values at other locations will be much greater in deeper water than shallow water. To account for this inhomogeneity in the interpolation of data values, we adapt the kriging interpolation algorithm [e.g., *Cressie*, 1990] by making the covariance function depth dependent, linearly transitioning between the two sets of model parameters shown in Figure 10 over the depth range 15–25 m. This same model is used for the kriging step of the maximum a posteriori resampling algorithm (equation (9)). The maximum a posteriori resampling algorithm had a run time of ~2 min on a Sun Ultra 10 workstation. The kriged interpolation of the resampled values is shown in Figure 11, along with the residual values indicating the difference between the pre-resampled (Figure 2a) and post-resampled images.

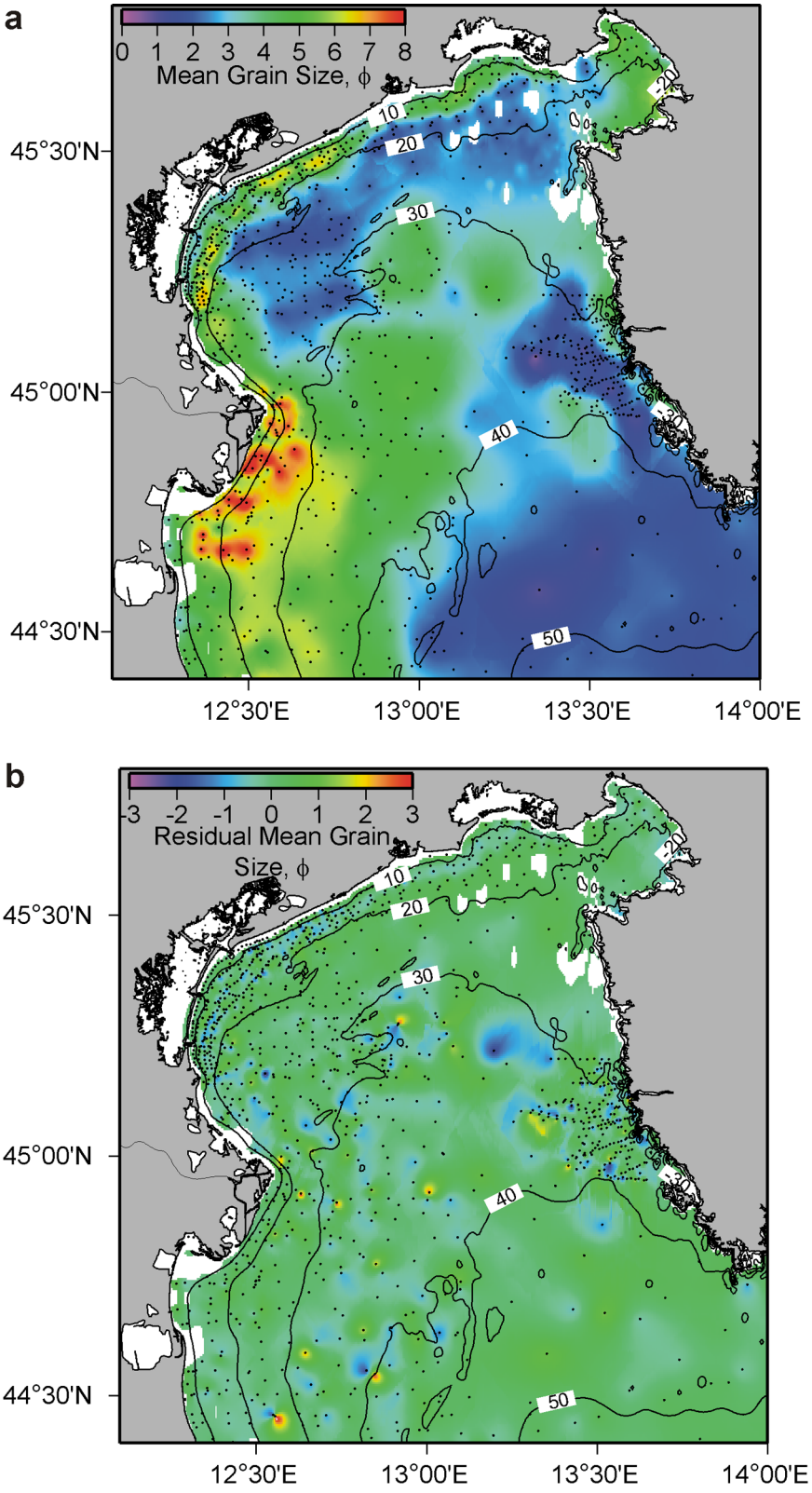

Figure 11. (a) Color-contoured interpolation of Adriatic Sea mean grain size data (Figure 2a) after maximum a posteriori resampling. Interpolation is accomplished through a modified version of the kriging algorithm (see text). Black dots indicate locations of data. Location shown in Figure 2b. (b) Color-contoured residual between pre-resample (Figure 2a) and post-resample (Figure 11a) interpolated images of the Adriatic Sea mean grain size data.

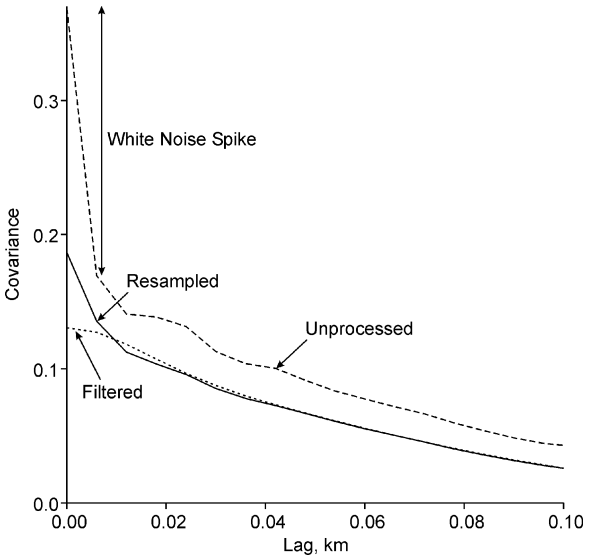

Figure 12. Covariance functions computed for the Martha's Vineyard Coastal Observatory acoustic backscatter data in the east-west direction, including unprocessed (Figures 3a and 13a), resampled (Figure 13b), and filtered (Figure 13c) images. See text for discussion.

[32] The interpolation of pre-resampled data in Figure 2a exhibits numerous dimple artifacts caused by large differences in data values that are proximal to each other. Both positive and negative dimples are prominent. The post-resampled image (Figure 11) shows these artifacts to be mostly removed, especially in the deeper waters (>20 m) where the correlation scale is much larger. The post-resampled image provides a more realistic and satisfactory presentation of the data in this case.

4.3. Martha's Vineyard Coastal Observatory Acoustic Backscatter

[33] The side-scan backscatter collected off the Martha's Vineyard Coastal Observatory [*Goff et al.*, 2004a] (Figure 3) is considered a fairly high quality data set for its kind. However, as is typical for acoustic backscatter, there is a high degree of speckly noise evident in the data. This is demonstrated quantitatively in Figure 12, where the east-west covariance function derived from the data is displayed: more than half the total data variance is taken up by the "white noise spike," which is the difference between the covariance at the 0th and 1st lag values. While correlation properties in the E-W direction, which is nearly the normal-to-strike direction, can be robustly estimated, the N-S direction is strongly influenced by track line artifacts, so some "expert guidance" is needed to estimate the along-strike correlation properties. The von Kármán parameters used for this example are: $H = 0.39$ (units are arbitrary measures of pixel strength), $\lambda_n = 0.18$ km, $\lambda_s = 0.51$ km, $\theta = 6°$, and $D = 2.5$. As derived from the covariance function in Figure 12, a uniform uncertainty of 0.47 was assumed for all data values. The data grid measures 437×255 with a node spacing of 6 m, and data fill every node point. The total number of data points resampled was over 111,000, and the run time for the maximum a posteriori resampling algorithm, incorporating the sector search algorithm for the 10 nearest resampled values for kriging, was ~2.25 hours on a Sun Ultra 10 workstation.

[34] Figure 13 presents a comparison between the unprocessed data (Figure 13a), the resampled data (Figure 13b), and filtered data (Figure 13c) operated on by a cosine filter with full width 0.045 km. More sophisticated filtering methods are available for reducing speckle noise (e.g., median or adaptive filters). However, our intent here is not to find the best possible filter, but rather to quantitatively demonstrate the differences between resampling and filtering in the simplest possible way. Filtering is straightforward to apply in this case, because the data fill the available grid space. Both the resampling and filtering greatly reduce the speckle noise. The filter length and shape are arbitrary; the image in Figure 13c could be made to look sharper or fuzzier, depending on these choices. However, this particular choice provides a unique opportunity to quantitatively compare the statistical effects of resampling and filtering, because the overall effect on the covariance at larger scales of these two methods is nearly identical (Figure 12). The difference between the two methods is manifest in the smaller lag scales, where the essential distinction between resampling and filtering is sharply defined. Filtering reduces noise by averaging, which flattens the shape of the covariance near the origin while also spreading some of the noise variance out to larger scales. In so doing, filtering has a potentially deleterious effect on the field in addition to reducing noise. Resampling, on the other hand, is able to more specifically target, although not entirely eliminate, the noise. The covariance function from the resampled data does not exhibit the flattened bulge near the origin that is characteristic of the filtered data, but rather is able to better retain the shape of the covariance function exhibited by the unprocessed data, albeit at overall reduced variance.

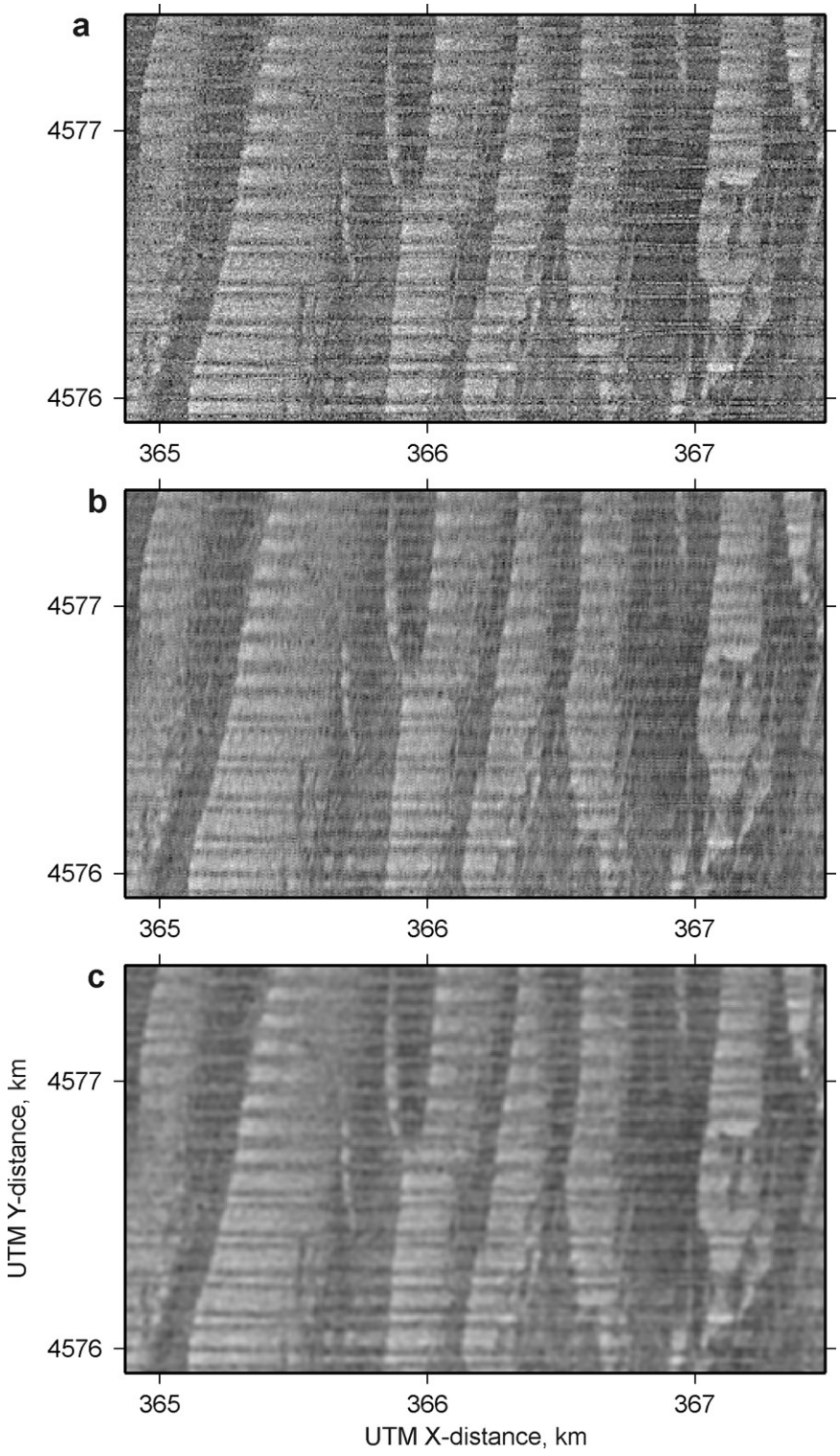

Figure 13. (a) Acoustic backscatter data for the survey of the Martha's Vineyard Coastal Observatory [*Goff et al.*, 2004a] (identical to Figure 3a). Lighter shades indicate higher backscatter intensity. Location shown in Figure 3b. (b) Data from Figure 13a after maximum a posteriori resampling. (c) Data from Figure 13a after filtering with a cosine function of full width 0.045 km.

[35] While the maximum a posteriori resampling algorithm may ultimately produce more satisfactory results than filtering, computer run time is a factor that may weigh heavily in favor of filtering: here, the filtering operation took less than 1 second, compared with ~2.25 hours for resampling on the same computer. Use of the maximum a posteriori resampling algorithm for large data sets will require cost/benefit considerations. However, more sophisticated nearest-neighbor search algorithms [e.g., *Samet*, 1990] could greatly alleviate such concerns. We will investigate such algorithms for future applications.

5. Conclusions

[36] The maximum a posteriori resampling algorithm presented in this paper has proven, in both synthetic tests and disparate data applications, to be a viable method for correcting noisy data where field values are spatially correlated but whose noise properties are largely white. The essential requirements for applying this method are a quantitative estimate of the uncertainty of the data and a characterization of the spatial covariance function for the sampled field. It should also only be employed where there is a clear expectation that changes in field parameters are gradational rather than abrupt. Potential applications are numerous. Maximum a posteriori resampling is an important alternative to filtering. Primary advantages include (1) an objective and optimal method for reducing noise and (2) better preservation of the statistical properties of the sampled field. The primary disadvantage is that maximum a posteriori resampling is a computationally expensive procedure. Application to large data sets will require cost/benefit considerations.

Acknowledgments

[37] The authors thank the following colleagues for helpful discussions on this project: Charles Holland, Barbara Kraft, Kevin Lepage, Larry Mayer, Bob Odom, Irina Overeem, Lincoln Pratson, and James Syvitski. Reviews by Alberto Malinverno and Christopher Small helped to improve the text in revision. This work has been supported by the Office of Naval Research under grants N0014-01-1-0891 and N00014-05-1-0701 (J.A.G.), N00014-01-1-0376, N00014-02-1-0432, and N00014-05-1-0080 (C.J.J.), and N00014-00-1-0092 (B.C.). UTIG contribution 1821.

References

Adler, R. J. (1981), *The Geometry of Random Fields*, 280 pp., John Wiley, Hoboken, N. J.

Cacchione, D. A., W. D. Grant, and G. B. Tate (1984), Rippled scour depressions on the inner continental shelf off central California, *J. Sediment. Petrol.*, *54*, 1280–1291.

Calder, B. (2006), On the uncertainty of archive hydrographic data sets, *IEEE J. Ocean Eng.*, in press.

Cressie, N. (1990), The origins of kriging, *Math. Geol.*, *22*, 239–252.

Deutsch, C. V., and A. G. Journel (1992), *GSLIB Geostatistical Software Library and User's Guide*, 340 pp., Oxford Univ. Press, New York.

Feller, W. (1971), *An Introduction to Probability Theory and Its Applications*, vol. 2, 669 pp., John Wiley, Hoboken, N. J.

Goff, J. A., and T. H. Jordan (1988), Stochastic modeling of seafloor morphology: Inversion of Sea Beam data for second-order statistics, *J. Geophys. Res.*, *93*, 13,589–13,608.

Goff, J. A., D. J. P. Swift, C. S. Duncan, L. A. Mayer, and J. Hughes-Clarke (1999), High resolution swath sonar investigation of sand ridge, dune and ribbon morphology in the offshore environment of the New Jersey Margin, *Mar. Geol.*, *161*, 309–339.

Goff, J. A., L. A. Mayer, P. Traykovski, I. Buynevich, R. Wilkens, R. Raymond, G. Glang, R. L. Evans, H. Olson, and C. Jenkins (2004a), Detailed investigation of sorted bedforms, or "rippled scour depressions," within the Martha's Vineyard Coastal Observatory, Massachusetts, *Cont. Shelf Res.*, *209*, 147–172.

Goff, J. A., B. J. Kraft, L. A. Mayer, S. G. Schock, C. K. Sommerfield, H. C. Olson, S. P. S. Gulick, and S. Nordfjord (2004b), Seabed characterization on the New Jersey middle and outer shelf: Correlability and spatial variability of seafloor sediment properties, *Mar. Geol.*, *209*, 147–172.

Jakobsson, M., B. Calder, and L. Mayer (2002), On the effect of random errors in gridded bathymetric compilations, *J. Geophys. Res.*, *107*(B12), 2358, doi:10.1029/2001JB000616.

Jenkins, C. J. (1997), Building offshore soils databases, *Sea Technol.*, *38*, 25–28.

Menke, W. (1989), *Geophysical Data Analysis: Discrete Inverse Theory*, revised edition, 289 pp., Elsevier, New York.

Murray, A. B., and E. R. Thieler (2004), A new hypothesis for the formation of large-scale inner-shelf sediment sorting and 'rippled scour depressions', *Cont. Shelf Res.*, *24*, 295–315.

Samet, H. (1990), *The Design and Analysis of Spatial Data Structures*, 493 pp., Addison-Wesley, Boston, Mass.

Smith, W. H. F., and P. Wessel (1990), Gridding with continuous curvature splines in tension, *Geophysics*, *55*, 293–305.

Taylor, H. M., and S. Karlin (1984), *An Introduction to Stochastic Modeling*, 399 pp., Elsevier, New York.

Weerasinghe, C., A. W.-C. Liew, and H. Yan (2002), Artifact reduction in compressed images based on region homogeneity constraints using the projection onto convex sets algorithm, *IEEE Trans. Circuits Syst. Video Technol.*, *12*, 891–897.

Williams, S. J., et al. (2003), New digital geologic maps of U. S. continental margins: Insights to seafloor sedimentary character, aggregate resources and processes, paper presented at Coastal Sediments '03 Conference Proceedings, Fifth International Symposium on Coastal Engineering and Science of Coastal Sediment Processes, Crossing Disciplinary Boundaries, East Meets West Prod. (EMW) Inc., Clearwater Beach, Fla., 18–23 May.